Journal of Radiation Research and Applied Sciences 17 (2024) 101123

Contents lists available at ScienceDirect

Journal of Radiation Research and Applied Sciences

journal homepage: www.journals.elsevier.com/journal-of-radiation-research-and-applied-sciences

Synthesis and characterization of metakaolin-based geopolymers doped with CRT waste glass for radiation shielding applications

M.S. Al-Buriahi [a,*], Mine Kırkbınar [b], Z.A. Alrowaili [c], Khadijah Mohammedsaleh Katubi [d], Norah Salem Alsaiari [d], Amani Alalawi [e], Norah Alomayrah [f], I.O. Olarinoye [g]

[a] Department of Physics, Sakarya University, Sakarya, Turkey
[b] Department of Nanotechnology Engineering, Faculty of Engineering, İstanbul Gedik University, İstanbul, Turkey
[c] Department of Physics, College of Science, Jouf University, P.O.Box:2014, Sakaka, Saudi Arabia
[d] Department of Chemistry, College of Science, Princess Nourah bint Abdulrahman University, P.O. Box 84428, Riyadh, 11671, Saudi Arabia
[e] Department of Physics, Faculty of Applied Science, Umm AL-Qura University, Al Taif Road, Makkah, 24382, Saudi Arabia
[f] Department of Physics, College of Science, Princess Nourah bint Abdulrahman University, P.O. Box 84428, Riyadh, 11671, Saudi Arabia
[g] Department of Physics, School of Physical Sciences, Federal University of Technology, Minna, Nigeria

ARTICLE INFO

Keywords:
Metakaolin geopolymers
CRT glass
Radiation shielding
Gamma dose

ABSTRACT

This study presents the influence of CRT glass on the gamma-ray interaction processes in metakaolin-based geopolymers. Four batches of G-CRT composites (namely, G, G-10CRT, G-20CRT, and G-30CRT, which represent geopolymer (G) samples doped with 0, 10, 20, and 30 wt% of CRT glass) were prepared using the cold hydrostatic press method. The mass attenuation coefficients of the prepared C-xCRT samples were computed using XCOM and FLUKA simulations for photons within the energy range of 15 keV–15 MeV. The density of the pristine geopolymer increased from about 1.86 g/cm^3 to 2.09, 2.26, and 2.34 g/cm^3 for G-10CRT, G-20CRT, and G-30CRT, respectively. The photon mass and linear attenuation coefficients of the geopolymers increased with CRT glass concentration. The half-value layer and mean free path were within the ranges 0.070–18.079 cm and 0.101–26.083 cm for G; 0.036–15.110 cm and 0.052–21.799 cm for G-10CRT; 0.024–13.197 cm and 0.014–19.039 cm for G-20CRT; and 0.018–12.074 and 0.026–17.419 cm for G-30CRT. The G-30CRT had the best gamma attenuating prowess in contrast to other G-xCRT. CRT-rich G-xCRT had a higher effective atomic number. For 10 mm thick geopolymer, the absorbed dose rates were 0.211 μR/h, 0.66 μR/h, 1.11 μR/h, and 1.55 μR/h for G, G-10CRT, G-20CRT, and G-30CRT, respectively, for 100 keV photons. The introduction of CRT glass into the geopolymer matrix improved their photon interaction cross-section. The geopolymers showed outstanding photon interaction ability compared to ordinary concrete and some shielding glasses at low photon energies. The CRT glass-doped geopolymer samples are useful for preparing radiation shielding concrete.

1. Introduction

Gamma photons are a key part of modern techniques involved in the control and management of diseases in man, animals and plants (El-Ghazaly et al., 2020; Katiyar et al., 2022; Ogundare et al., 2008). In addition, many industries utilize photons for many applications such as for food production and preservation, environmental conservation, non-destructive tests and quality assurance processes in material fabrication, and petroleum product exploration and transportation (Hornitzky, 1994; Madureira et al., 2020; Pricaz & Uţă, 2015; Roshani et al., 2021). As important as gamma radiation is to human society, its applications come with risks to living and nonliving components of the environment. Research has shown that the exposure of gamma photons to biological tissues and nonbiological materials produces undesirable effects. Gamma rays are high-energy photons that can produce excitation, ionization and displacement of atoms in a system. These effects can lead to changes in the properties and functionalities of a biological cell or nonliving material (Ali et al., 2015; Allen et al., 1960; Kang et al., 2023; Mansour et al., 2024; Mikhalkevich et al., 2021; Mohamed et al., 2024; Vucic et al., 2006). While some of the changes are desirable when radiation exposure is controlled (Mansour et al., 2024; Mohamed et al., 2024) uncontrolled exposure can be destructive (Kang et al., 2023). The extent of the induced changes is mostly dependent on energy and the period of irradiation. The fact that gamma radiation is present due to

* Corresponding author.
E-mail address: alburiahi@sakarya.edu.tr (M.S. Al-Buriahi).

https://doi.org/10.1016/j.jrras.2024.101123
Received 4 August 2024; Received in revised form 12 September 2024; Accepted 18 September 2024
Available online 21 September 2024

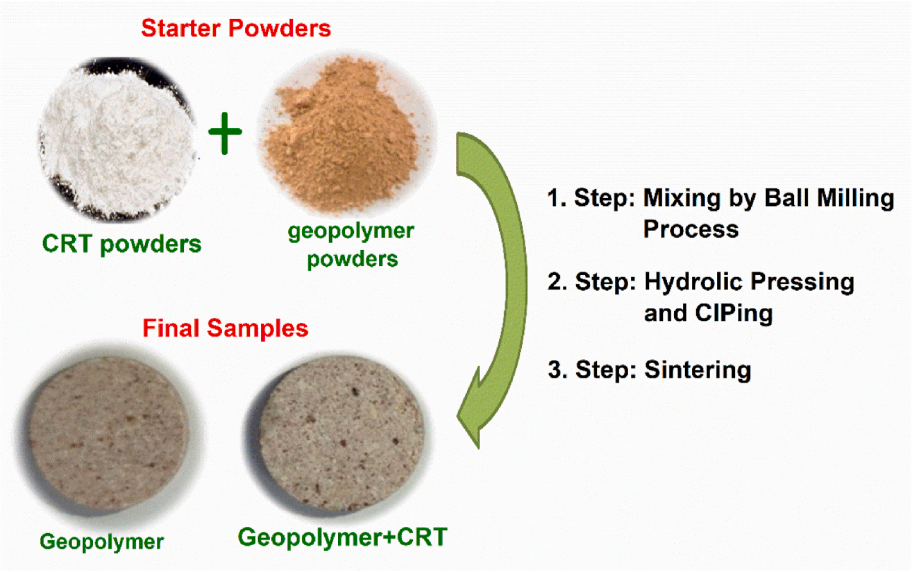

Fig. 1. The production process of the CRT glass infused geopolymer composite.

Table 1
Sample code and weight fraction (wt.%) of element present the prepared G-*x*CRT glasses including their measured density.

Element	Glass sample			
	G	G-10CRT	G-20CRT	G-30CRT
O	0.5202	0.4726	0.4553	0.4381
Na	0.0304	0.0579	0.0551	0.0523
Mg	0	0.0011	0.0021	0.0034
Al	0.1768	0.1606	0.1447	0.1281
Si	0.2726	0.2668	0.2606	0.2546
K	0	0.0035	0.0069	0.0104
Ca	0	0.0012	0.0025	0.0037
Fe	0	0.0005	0.0012	0.0018
Sr	0	0.0013	0.0025	0.0038
Ba	0	0.0006	0.0013	0.0021
Pb	0	0.0339	0.0678	0.1017
Density (g/cm3)	1.86 ± 0.08	2.09 ± 0.05	2.26 ± 0.06	2.34 ± 0.07

natural radioactive processes in space and on the Earth as well as from man-made processes involving radiation applications, exposure may be inevitable. However, deliberate control of exposure is important to mitigate the unwanted radiation-induced effects on man, animals, gadgets, and the environment at large. Such control is meant to eliminate the possibility of the occurrence of unwanted radiation-induced defects with dose thresholds and reduce the probabilities of occurrence of those without dose outset.

The use of shields is a widely accepted method of radiation protection. Many materials including different species of concrete, natural rocks, alloys, ceramics, and glasses have been used for shielding in different situations (Al-Buriahi et al., 2021a; Al- et al., 2022a; Alshahrani et al., 2021; Alshahrani et al., 2022; Ardiansyah et al., 2023; Güler et al., 2024; Günoğlu et al., 2024; Kang et al., 2023). Concrete is the most common among these materials due to its availability and cost-effectiveness relative to other materials. The use of concrete as a building material in radiation facilities thus serves dual purposes-as a shield and structural material. In recent times, the environmental cost of sourcing raw materials for making cement (the main binder in concrete) has become obvious (Mansoori et al., 2023; Zhang et al., 2023). Sourcing for alternative materials for partially replacing cement in concrete making is therefore an interesting aspect of research from an environmental conservation perspective.

Using geopolymers as partial substitutes for cement is an environmentally friendly and cost-effective way of producing concrete (Alrowaili, Alnairi, et al., 2023; Asghar et al., 2023; Hwalla et al., 2023; Nawaz et al., 2020; Zhang et al., 2023; Ślosarczyk et al., 2023). The use of geopolymer and its effect on the general properties of concrete has been investigated previously (Alrowaili, Alnairi, et al., 2023; Asghar et al., 2023; Hwalla et al., 2023; Mansoori et al., 2023; Nawaz et al., 2020; Zhang et al., 2023; Ślosarczyk et al., 2023). The results have shown that geopolymers, especially from industrial and agricultural waste products such as fly ash and rice husk ash improve concrete mechanical properties (Fernando et al., 2023; Hwang & Huynh, 2015; Zhang et al., 2023). In addition, producing geopolymers from waste products helps to keep the environment safer and cleaner. Furthermore, the use of geopolymers should enhance the radiation shielding efficiency of concrete. This is important for radiation-shielding concrete. Recently, the gamma-radiation interaction parameters of some geopolymers were investigated (Alrowaili, Alnairi, et al., 2023; Zhang et al., 2023), and it was ascertained that they have high gamma-ray interaction cross-sections compared to some existing shielding materials. The use of such geopolymers is therefore desirable in improving the radiation shielding performance of concrete.

The advent of modern technology in display systems has prevented the closed-loop recycling of waste cathode ray tube (CRT) glasses (CG). Hence, CG glass accumulates in the environment as unwanted materials. CRT glasses contain heavy elements such as Ba, Pb, Sr, Sb, and Zr (Alrowaili, Alzahrani, et al., 2023). Previous studies have shown that the presence of these elements makes CG an important gamma-shielding material (Al- et al., 2022b; Al- et al., 2023; Alrowaili, Alzahrani, et al., 2023; Basha et al., 2024). In an attempt to provide an eco-friendly alternative to concrete materials, Gorski et al. (Górski et al., 2021) investigated the influence of metakaolin-based geopolymer infused with CG as aggregate on the mechanical properties of concrete. The study deduced that an optimum CG concentration of 50% by weight produced the highest mechanical strength. In addition, an analysis of the aqueous extract showed that it contained lower toxic heavy metals when the CG was well embedded in the geopolymer matrix. Ogundiran et al. (Ogundiran & Enakerakpo, 2018) also affirmed that the addition of CG to metakaolin clay geopolymer improved the density and mechanical attributes and reduced the toxic metal leaching from the geopolymer to an environmentally safe level. Similarly, other recent studies (Gao et al., 2022; Guzmán-Carrillo et al., 2021; Long et al., 2022) have shown that the encapsulation of CG in geopolymers is an effective and sustainable way of recycling CG and producing an efficient binder for concrete.

Table 2
Mass attenuation coefficient of the prepared G-*x*CRT glasses via FLUKA and XCOM at different photon energies.

E (MeV)	G			G-10CRT			G-20CRT		
	XCOM	FLUKA	Dev.%	XCOM	FLUKA	Dev.%	XCOM	FLUKA	Dev.%
0.015	5.32165	5.27349	0.905	9.18084	9.11080	0.147	9.18084	9.11080	0.763
0.02	2.33790	2.35819	0.868	5.37018	5.37810	0.187	5.37018	5.37810	0.147
0.03	0.80947	0.80934	0.016	1.86834	1.87184	0.181	1.86834	1.87184	0.187
0.04	0.43814	0.43727	0.199	0.94771	0.94599	1.525	0.94771	0.94599	0.181
0.05	0.30408	0.29507	2.962	0.58651	0.57756	2.950	0.58651	0.57756	1.525
0.06	0.24264	0.23588	2.783	0.41655	0.40426	0.020	0.41655	0.40426	2.950
0.08	0.18918	0.19518	3.168	0.26998	0.26993	0.236	0.26998	0.26993	0.020
0.1	0.16569	0.16615	0.281	0.35085	0.35168	0.141	0.35085	0.35168	0.236
0.15	0.13870	0.13919	0.353	0.20303	0.20332	1.128	0.20303	0.20332	0.141
0.2	0.12438	0.12646	1.678	0.15426	0.15600	1.045	0.15426	0.15600	1.128
0.3	0.10669	0.10805	1.278	0.11674	0.11796	0.506	0.11674	0.11796	1.045
0.4	0.09516	0.09588	0.757	0.09975	0.10026	0.660	0.09975	0.10026	0.506
0.5	0.08673	0.08748	0.854	0.08919	0.08978	0.076	0.08919	0.08978	0.660
0.6	0.08014	0.08016	0.024	0.08158	0.08152	0.490	0.08158	0.08152	0.076
0.8	0.07033	0.07076	0.605	0.07087	0.07122	0.148	0.07087	0.07122	0.490
1.0	0.06321	0.06315	0.080	0.06340	0.06330	0.506	0.06340	0.06330	0.148
1.5	0.05146	0.05151	0.079	0.05143	0.05117	0.477	0.05143	0.05117	0.506
2	0.04436	0.04417	0.431	0.04437	0.04416	0.899	0.04437	0.04416	0.477
3	0.03606	0.03575	0.850	0.03625	0.03593	0.934	0.03625	0.03593	0.899
4	0.03137	0.03108	0.927	0.03174	0.03144	0.903	0.03174	0.03144	0.934
5	0.02839	0.02812	0.932	0.02890	0.02863	0.715	0.02890	0.02863	0.903
6	0.02635	0.02617	0.684	0.02698	0.02679	0.356	0.02698	0.02679	0.715
8	0.02380	0.02375	0.223	0.02464	0.02456	0.301	0.02464	0.02456	0.356
10	0.02234	0.02231	0.137	0.02335	0.02328	0.454	0.02335	0.02328	0.301
15	0.02061	0.02054	0.337	0.02195	0.02185	0.147	0.02195	0.02185	0.454

Energy (MeV)	G-20CRT			G-30CRT		
	XCOM	FLUKA	Dev.%	XCOM	FLUKA	Dev.%
0.015	12.96720	12.87503	0.711	16.75440	16.57383	1.078
0.02	8.36721	8.37065	0.041	11.37019	11.39576	0.225
0.03	2.91707	2.92051	0.118	3.96787	3.96866	0.020
0.04	1.45516	1.45280	0.162	1.96557	1.96244	0.159
0.05	0.86806	0.85845	1.107	1.15127	1.14033	0.950
0.06	0.59008	0.58242	1.298	0.76461	0.75622	1.098
0.08	0.35075	0.34877	0.563	0.43197	0.42848	0.810
0.1	0.53609	0.53690	0.150	0.72158	0.72191	0.046
0.15	0.26749	0.26734	0.055	0.33203	0.33152	0.155
0.2	0.18429	0.18571	0.774	0.21435	0.21550	0.539
0.3	0.12692	0.12796	0.819	0.13711	0.13807	0.699
0.4	0.10446	0.10484	0.367	0.10917	0.10946	0.258
0.5	0.09175	0.09215	0.435	0.09432	0.09469	0.393
0.6	0.08311	0.08299	0.151	0.08465	0.08449	0.190
0.8	0.07151	0.07185	0.473	0.07214	0.07241	0.372
1.0	0.06367	0.06353	0.217	0.06394	0.06375	0.287
1.5	0.05146	0.05118	0.536	0.05149	0.05119	0.581
2	0.04444	0.04421	0.505	0.04450	0.04426	0.550
3	0.03648	0.03614	0.937	0.03671	0.03636	0.962
4	0.03212	0.03182	0.925	0.03250	0.03220	0.934
5	0.02941	0.02917	0.809	0.02993	0.02968	0.829
6	0.02762	0.02744	0.633	0.02825	0.02807	0.627
8	0.02547	0.02537	0.384	0.02630	0.02620	0.362
10	0.02433	0.02424	0.368	0.02532	0.02523	0.346
15	0.02324	0.02316	0.330	0.02453	0.02446	0.312

Since concrete is a basic shielding material, and the fact that an empirical investigation of the influence of CG on the gamma absorbing efficiency of geopolymers is scanty in the literature, it has become imperative to investigate how the introduction of CG influences the photon interaction competence of geopolymers.

In the present study, metakaolin-based geopolymer was infused with CG to improve the gamma interaction prowess of the geopolymer (G). This study was motivated by the need to keep the environment cleaner and safer through the recycling of waste products (in this case CRT glass). In addition, the use of geopolymer for producing radiation shielding concrete would reduce the amount of cement used for concrete making. This would also cut the amount of greenhouse gases, and atmospheric dust released during cement production, and mitigate ecological problems associated with sourcing for raw materials for making cement and concrete. The research is important from a radiation protection standpoint, as it investigates the possibility of using G and CG composite for green radiation shielding concrete.

2. Materials and methods

2.1. Preparation of geopolymer-CRT glass composite

An out-of-use CRT of a colored TV was obtained from a local waste management and recycling company in Turkey. The CG was already separated from other components of the CRT, such as metals and plastic. The CG was obtained in crushed form. The crushed CG was crushed further into homogenous powder using a vibratory mill that was operated at 3000 rps speed. The obtained fine and consistent powder was added to a reference geopolymer (G) powder. The geopolymer was a metakaolin-based geopolymer activated with NaOH. The metakaolin

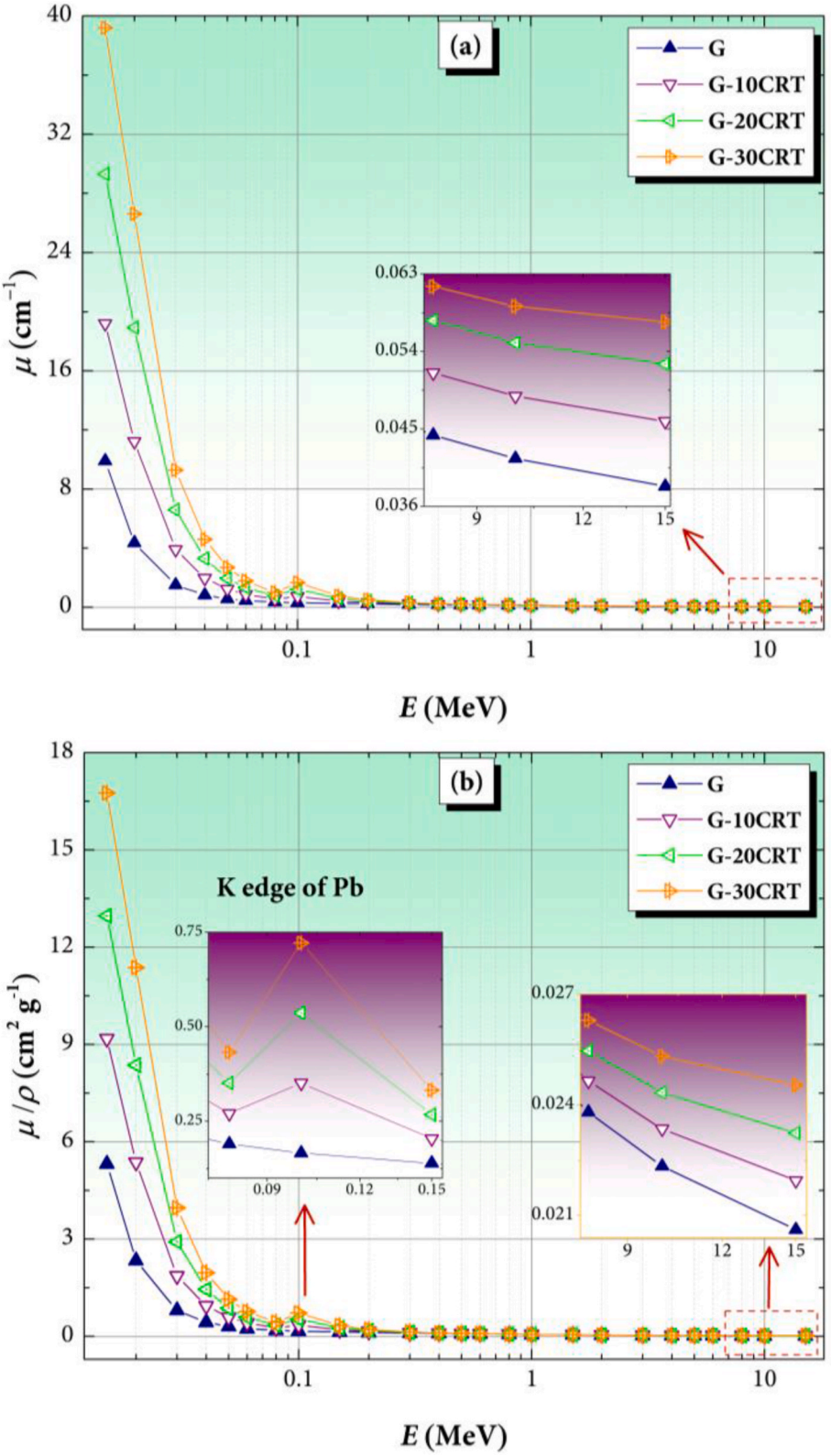

Fig. 2. Variations of (a) linear attenuation coefficient and (b) mass attenuation coefficient of the prepared G-*x*CRT.

was prepared from kaolin rock calcined at 650 °C for 4 h. A mixture of the metakaolin and NaOH in the weight proportion of 80 wt% and 20 wt %, respectively, was well mixed and ground in a ring mill to give the geopolymer. Four batches of G-CG mixtures (namely, G, G-10CRT, G-20CRT, and G-30CRT, which represent geopolymer (G) samples doped with 0, 10, 20, and 30 wt% of CG powder) were prepared using the cold hydrostatic press. Each sample was pressed under hydraulic pressing in a steel mold under 250 MPa pressure. All samples were then calcined at 1000 °C for 1 h in order to obtain bulk material. The production process of the CRT glass infused geopolymer composite is illustrated in Fig. 1. The bulk densities of the prepared samples were determined through the Archimedes method, with distilled water serving as the buoyancy liquid.

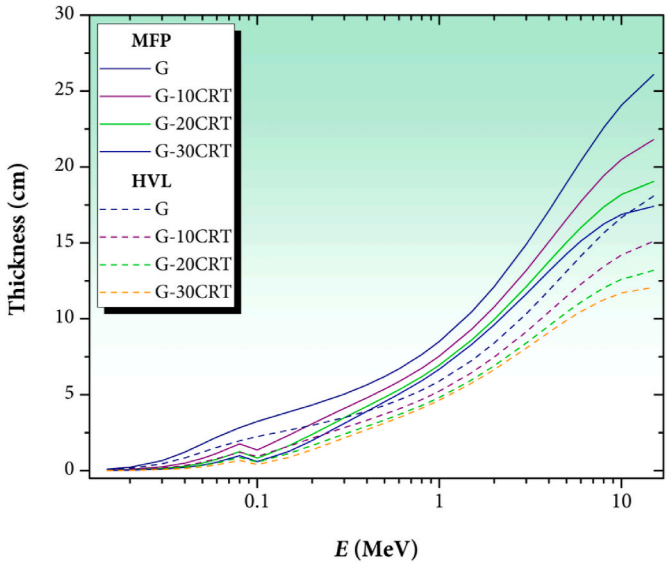

Fig. 3. Variation of thickness in terms of mean free path (MFP, solid line) and half value layer (HVL, dash line) with respect to a function of photon energy in the prepared G-*x*CRT samples.

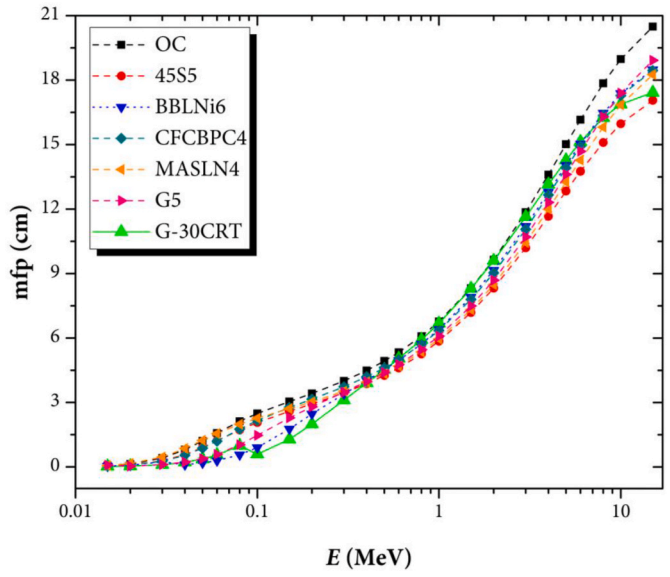

Fig. 4. Comparison of mean free path (mfp) of the prepared G-30CRT sample with those in radiation shielding materials such as ordinary concrete (OC) (Bashter, 1997), 45S5 (Al-Buriahi et al., 2021), BBLNi6 (Al-Buriahi et al., 2020), CFCBPC4 (Al- et al., 2022c), MASLN4 (Alothman et al., 2022), and G5 (Shaaban et al., 2019) glasses.

All weight measurements and other procedures in the Archimedes technique were conducted at room temperature. The chemical composition of the G-xCRT samples was determined by X-ray fluorescence (XRF) spectrometry.

2.2. Brief theory about photon transmission

Photons are the most commonly encountered form of ionizing radiation in industries; in addition, they are emitted in the interactions and release of other forms of ionizing radiation. An understanding of photon interaction processes and energy deposition in matter is important for radiation processing and the control of irradiation processes. The interaction of photons with materials can be summarized using distinct

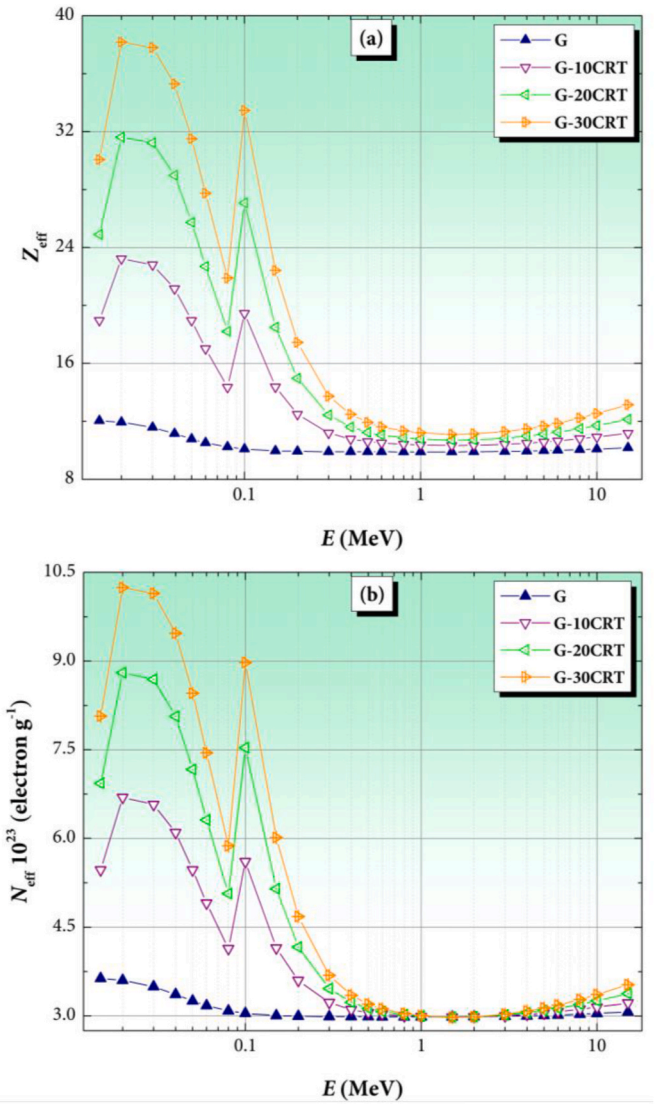

Fig. 5. Variations of (a) effective atomic number and (b) effective electron density of the prepared G-*x*CRT glasses, with different photon energies.

interaction parameters. These parameters are crucial for the assessment of photon transmission and energy deposition processes. Generally, the ratio of the density of transmitted ($T(E)$) to incident ($I(E)$) photon flux through a material of thickness (x) can be summarized using the remodeled Beer-Lambert equation (Olarinoye, 2017; Olarinoye et al., 2019)(Olarinoye, 2017; Olarinoye et al., 2019).

$$\frac{T(E)}{I(E)} = B(E,\lambda)\exp\left(-\mu_m \rho x\right) \quad (1)$$

This equation shows that the photon transmission efficiency of a medium depends on the energy of photons and the material's characteristics, namely, thickness, density (ρ), mass attenuation coefficient (μ_m), and photon buildup competence B. The energy of photons determines the interaction and energy deposition processes that can lead to low photon transmission (or attenuation). The value of μ_m is an important quantity for comparing how well a material interacts with photons. It can be used to directly obtain other important interaction parameters. The linear attenuation coefficient μ is similar to μ_m but changes with material thickness, unlike μ_m which is normalized for density. They are both related as $\mu_m = \frac{\mu}{\rho}$. The value of $B(E,x)$ represent a multiplier which is used to convert narrow beam to broad beam transmission. For narrow beam transmission, $B(E,x)$ is unity, and the value of μ can be obtained

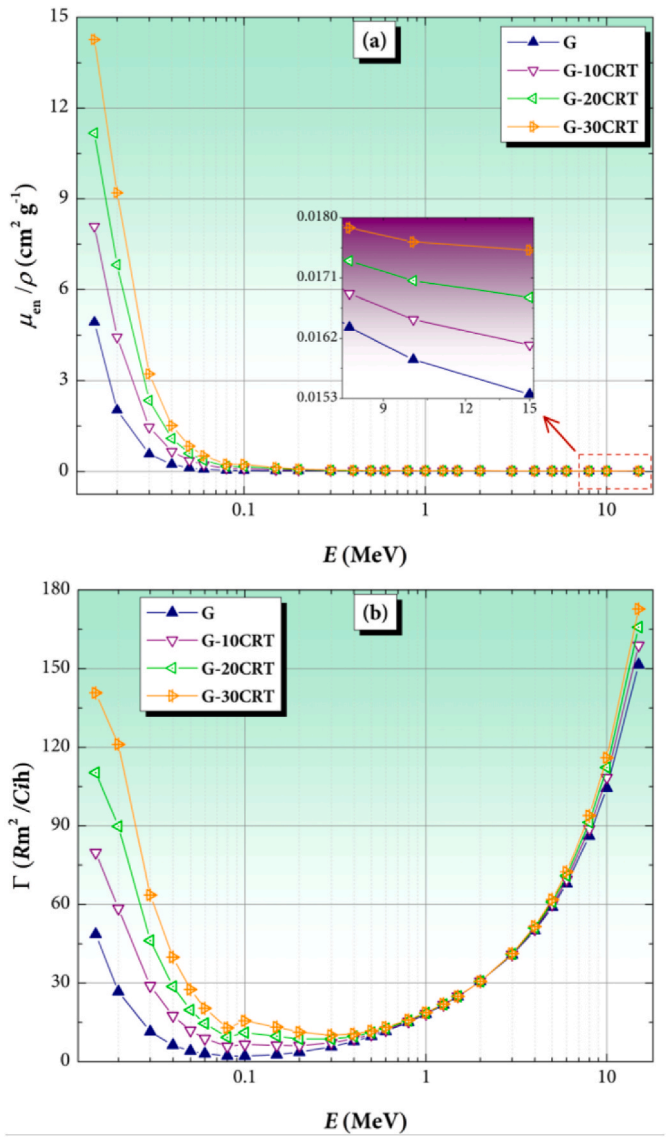

Fig. 6. Variations of (a) mass energy-absorption and (b) specific gamma-ray constant of the prepared G-*x*CRT glasses, with different photon energies.

from experimental or simulation data base on the rearrangement of Equation (1) as:

$$\frac{\ln\left(I(E)/T(E)\right)}{x}=\mu \tag{2}$$

Alternatively, μ or μ_m can be evaluated theoretically using photon cross-section data library, such as XCOM or its window version WinXCOM (Berger & Hubbell, 1987; Gerward et al., 2004). Values of μ_m and μ determined through experiments and simulations are often compared with those from XCOM to validate the narrow beam geometry used for the experiment or simulation.

2.3. Determination of μ_m and associated parameters

The values of μ_m was computed for the CRT impregnated G samples using XCOM and FLUKA simulations for photons within the energy range 15 keV-15 MeV. Using the chemical composition of the G-xCRT samples as input parameters in XCOM, μ_m for 25 discrete photon energies was computed. For the FLUKA simulations, the input file card includes the BEAM and BEAMPOS card which contains the description of the photon source, position, and energy, the MATERIAL card contains the description of the absorbing material and geometry. The void which is the region that host the source and setup geometry was surrounded by a black hole that serves as a sink for photons around the simulation setup. Details of adopted FLUKA geometry and simulation method can be found in previous studies (Al- et al., 2021b; Katubi et al., 2022). The values of μ_m obtained from FUKA was compared to those from XCOM by computing the relative differences (in %) between both datasets. To understand the photon interaction processes and highlight the evolution in the photon absorption prowess of each G-XCRT, other photon interaction parameters were computed based on the following expressions (Alzahrani et al., 2023):

$$\text{Mean free path}: mfp\ (cm)=\frac{1}{\mu\ (cm^{-1})} \tag{3}$$

$$\text{Half}-\text{value layer}: HVL\ (cm)=\frac{ln\ 2}{\mu\ (cm^{-1})} \tag{4}$$

$$\text{Effective atomic number}: Z_{eff}=\frac{\sum_i (WF)_i A_i \left(\frac{\mu}{\rho}\right)_i}{\sum_i (WF)_i \frac{A_i}{Z_i}\left(\frac{\mu}{\rho}\right)_i} \tag{5}$$

$$\text{Effective electron density}: N_{eff}=\frac{N_A Z_{eff}}{\langle A\rangle} \tag{6}$$

The photon energy absorption related parameters were also computed for the G-xCRT samples. These evaluated parameters include mass energy absorption coefficients $\left(\mu_{en}/\rho\right)$, specific gamma constant (Γ), and absorbed gamma dose rate (D_r).

The energy absorption (EABF) and exposure (EBF) buildup factors for the materials were also calculated for material depths (x) up to 40 mfp using the geometric progression (GP) fitting method as highlighted in Equations (7)–(9) (Almuqrin et al., 2021; Yoshida, 2006):

$$\frac{EABF}{EBF(E,x)}=1+\frac{(b-1)(K^x-1)}{K-1}\ \text{for}\ K\neq 1 \tag{7}$$

$$\frac{EABF}{EBF(E,x)}=1+(b-1)x\ \text{for}\ K=1 \tag{8}$$

$$K(E,x)=cx^a+d\frac{\tanh\left(x/X_\kappa-2\right)-\tanh(-2)}{1-\tanh(-2)} \tag{9}$$

3. Results and discussion

3.1. Chemical composition and density of G and G-xCRT samples

The weight concentrations of the different atoms contained in the pristine geopolymer and those mixed with CRT (as revealed by the XRF analysis) and densities of the geopolymers are displayed in Table 1. The pristine geopolymer (G) contained mainly four atoms in varying proportions (O, Na, Al, and Si). This indicated the presence of oxides of Na, Al, and Si in G with SiO_2 having the highest concentration. The introduction of CRT into the G matrix decreased the weight concentrations of all the four atomic species initially in G. This is a result of the presence of heavier atoms including Ba, Pb, and Sr present in the introduced CRT. Furthermore, the density of the pristine geopolymer increased from about 1.86 g/cm^3 to 2.09, 2.26, and 2.34 g/cm^3 for G-10CRT, G-20CRT, and G-30CRT, respectively. CRT contains heavy atoms and its density generally lies between 2.95 and 3.09 g/cm^3 (Bawab et al., 2021; Maschio et al., 2013). The bulk density of the introduced CRT was about 3.08 ± 0.05 which is higher than that of G. Therefore, the density of the composite geopolymer increases as the CRT content rises.

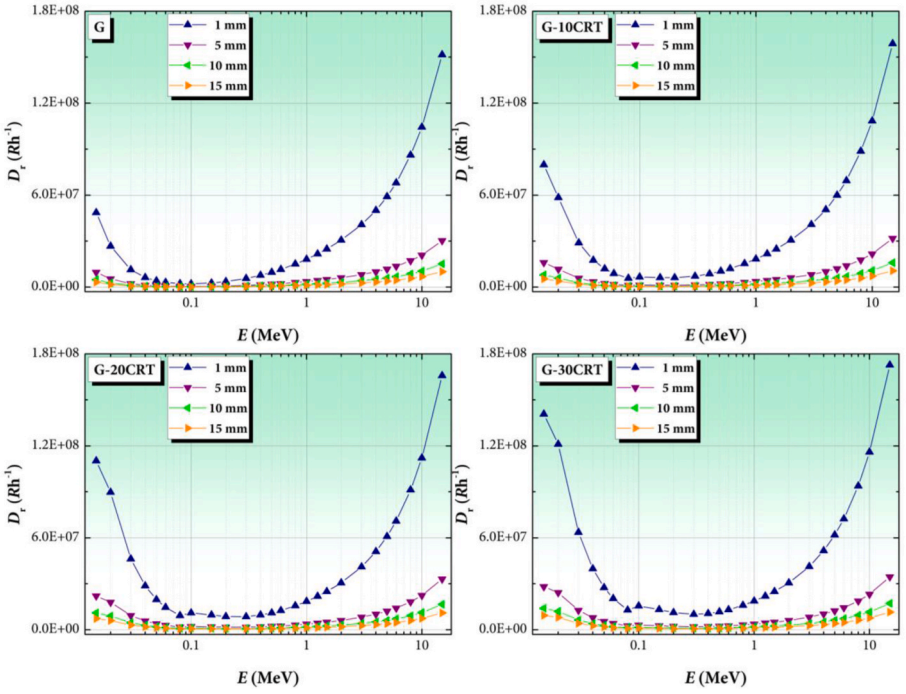

Fig. 7. Variation of gamma dose rate at different photon energy levels for the prepared G-*x*CRT glasses.

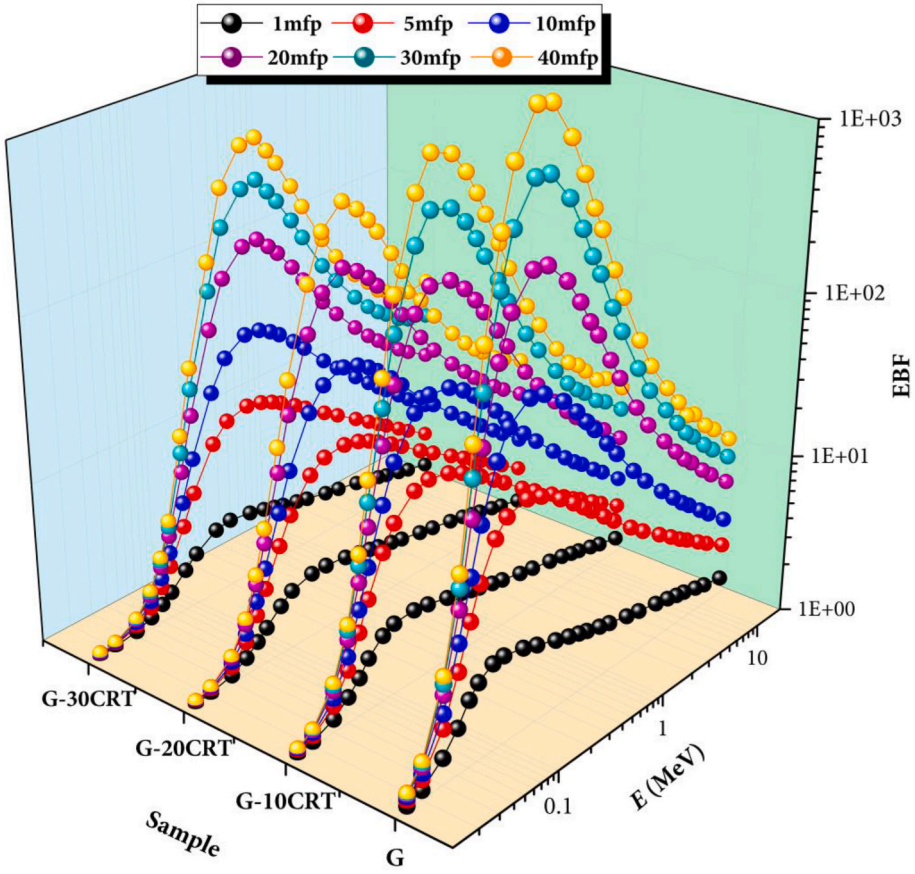

Fig. 8. Variation of energy absorption buildup factor (EBF) with the photon energy for the prepared G-*x*CRT glasses.

3.2. Mass and linear attenuation coefficients

The mass attenuation coefficient computed from XCOM and FLUKA simulations and the deviations between the two sets of μ_m are presented in Table 2. The absolute values of the deviations between the μ_m computed from XCOM and Monte Carlo simulations are within 3.20%.

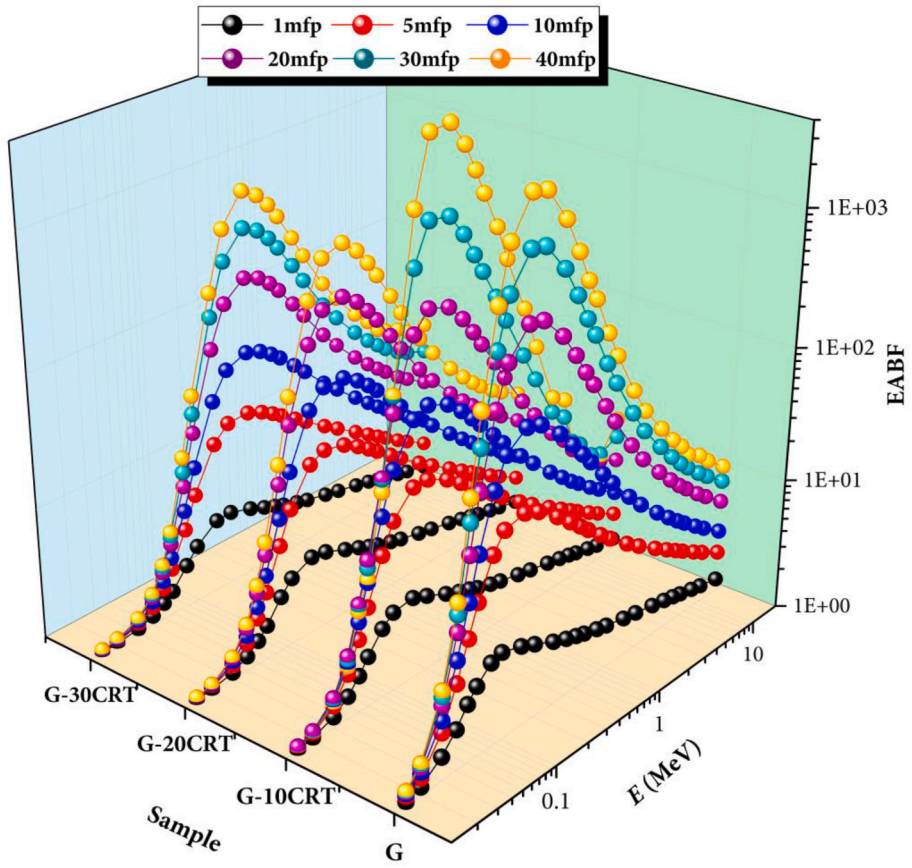

Fig. 9. Variation of energy absorption buildup factor (EABF) with the photon energy for the prepared G-*x*CRT glasses.

This shows that the simulation setup is approximately a narrow geometry. Hence, the FLUKA-generated μ_m are accurate and reliable. The changes in the attenuation coefficients (μ and μ_m) of the G and G-xCRT with respect to photon beam energy are displayed in Fig. 2 ((a) and (b), respectively). The linear and mass attenuation coefficients curves are similar and proportional. Consequently, both curves have the following common features: First, the attenuation coefficients increase with CRT concentration. Second, the coefficients decrease with incident photon energy at an initially rapid rate for energies below 60 keV, then slowly for the rest of the energy spectrum. Lastly, the decrease in the values of the attenuation coefficients was briefly disturbed at 100 keV, where μ and μ_m increase slightly except for pristine G. The increase in μ and μ_m as CRT content increases in the samples is attributed to the presence of heavy atoms including Ba, Pb, and Sr, whose concentrations are higher in CRT-rich samples. For a composite material, the addition rule (Equation (10)) can be used to obtain the value of μ and μ_m at each energy

$$\mu_m = \sum (WF)_i (\mu_m)_i \tag{10}$$

Therefore, the μ or μ_m of the samples depend on the weight fraction and μ or μ_m of the atoms in them. Due to the higher μ and μ_m and weight proportions of heavy atoms (Ba, Pb, and Sr) present in samples rich in CRT, G-xCRT containing higher CRT content had higher μ and μ_m. The energy behavior of the attenuation coefficients can be explained from the perspective of partial photon interaction cross-sections due to photoionization absorption (PIA) and Incoherent scattering (ICS). PIA occurs at low energies near absorption edges of atoms and also leads to the complete absorption of incident photons. On the other hand, ICS reduces the energy of the incident photon beams after scattering. Although, other photon interaction processes occur, these two are believed to significantly influence the energy response of μ and μ_m of G and G-xCRT. The microscopic cross-sections (σ_x)of PIA and ICS can be given as (Kaur et al., 2019):

$$\sigma_{PIA} \propto Z^5 / E_\gamma^{3.5} \tag{11}$$

$$\sigma_{ICS} \propto Z / E_\gamma A \tag{12}$$

where, E_γ is the incident photon energy and Z, the atomic number of the interacting atoms. Therefore, the initially high but rapidly decreasing values of μ and μ_m is a result of the dominance of PIA, while the later slow decrease is attributed to the significance of ICS. The unexpected rise in attenuation coefficients at 100 keV is attributed to the K-absorption edge of Pb. The K-edge of Pb is around 88 keV, the high photon absorption at this energy is believed to influence the high attenuation coefficients at 100 keV for G-xCRT samples.

3.3. *Half-value layer and mean free path*

The HVL and mfp are parameters used to describe photon interaction ability of a medium in terms of its thickness. While the HVL depicts the thickness required to attenuate 50% of incident photon beam, the mfp gives the mean distance moved between collision within the material. Both parameters are inversely proportional to the attenuation coefficients (as shown in Equations 3 and 4). The values of HVL and mfp for the G-CRT composites are plotted against photon energy in Fig. 3. The HVL and mfp are within the ranges 0.070–18.079 cm and 0.101–26.083 cm for G; 0.036–15.110 cm and 0.052–21.799 cm for G-10CRT; 0.024–13.197 cm and 0.014–19.039 cm for G-20CRT; and 0.018–12.074 and 0.026–17.419 cm for G-30CRT. Fig. 3 indicates that samples rich in CRT have lower HVL and mfp at all energies. This shows that they attenuate photons better. Thus, G-30CRT has the lowest HVL

and mfp while G had the highest for both parameters of all the four prepared materials. The increasing trend of HVL and mfp as energy increases is an indication of decrease in the scattering and absorption processes in the G-xCRT materials leading to high photon transmission, mfps and HVLs.

In Fig. 4, the gamma-ray attenuation capacity of G-30CRT is placed in contrast to ordinary concrete (OC) (Bashter, 1997), 45S5 (Al-Buriahi et al., 2021), BBLNi6 (Al-Buriahi et al., 2020), CFCBPC4 (Al- et al., 2022c), MASLN4 (Alothman et al., 2022), and G5 (Shaaban et al., 2019) glasses. The mfp of G-30CRT is lower than OCs for the entire energy spectrum. This shows that G containing 30 wt% of CRT can absorb 15 keV-15 MeV better than OC. Also, the mfp of G-30CRT is lower than other materials in Fig. 4 for gamma radiation energy below 60 keV. This indicates that G-30CRT has a better gamma attenuating prowess in contrast to these glasses at these energies.

3.4. Effective atomic number and electron density

Values of Z_{eff} and N_{eff} computed based on Equations (5) and (6) are displayed as functions of energy in Fig. 5(a) and (b), respectively. Z_{eff} is in the range 9.90–11.95, 10.34–23.22, 10.71–31.63, and 11.10–38.18, while the values of N_{eff} are within the range 2.98–3.63, 2.98–6.69, 2.98–8.80, and 2.98–10.24 $\times$ 10^{23} electron/g, for G, G-10CRT, G-20CRT, and G-30CRT, respectively. Due to higher mass attenuation coefficients, CRT-rich G-*x*CRT has higher Z_{eff} and N_{eff}. The K-absorption edge of Pb is responsible in the spike in Z_{eff} and N_{eff} at 1 MeV. Unlike the attenuation coefficients, Z_{eff} and N_{eff} values increase for gamma photon energy greater than 1.5 MeV. This is attributed to the sensitive nature of the two parameters to pair production process. The cross-section of the pair production process (PPP) increases with energy such that $\sigma_{PPA} \propto Z^2 \ln E_\gamma$. Materials containing atoms with greater atomic number absorbs photon better and hence, possess greater values of Z_{eff}.

3.5. Mass energy absorption coefficients, specific gamma constant and gamma dose rate

Mass energy absorption coefficient ($\frac{\mu_{en}}{\rho}$), specific gamma constant, Γ, and dose rate D_r are essential in estimating gamma energy deposited in a material. They are also useful for assessing and comparing energy dosimetry importance of different media. The variations in the values of $\frac{\mu_{en}}{\rho}$ and Γ with respect to energy are displayed in Fig. 6(a) and (b), respectively. The curves of $\frac{\mu_{en}}{\rho}$ and μ/ρ are similar, because of the direct relationship between them. Theoretically, the incident photon energy, absorbed energy E_{ab}, $\frac{\mu_{en}}{\rho}$, and μ/ρ are related as (Podgorsak, 2006):

$$\frac{\mu_{en}}{\rho} = \mu/\rho \frac{E_{ab}}{E_\gamma} \tag{13}$$

Consequently, the trend of $\frac{\mu_{en}}{\rho}$ and μ/ρ are essentially the same for the same reasons.

The energy response and trend of Γ can be explained according to the expression:

$$\Gamma \propto \frac{\mu_{en}}{\rho} E_\gamma \tag{14}$$

For $E_\gamma < 1\ MeV$, the energy response of Γ is dictated by μ/ρ while at greater energy, increasing trend is dictated by increasing E_γ and PPP. In Fig. 7, values of the absorbed doses D_r in 1 mm, 5 mm, 10 mm, and 15 mm thick G-*x*CRT material are displayed as a function of energy. Increasing geometric and exponential decay of photons in the geopolymers lower doses at greater depths. For 10 mm thick geopolymer, D_r is 0.211 μR/h, 0.66 μR/h, 1.11 μR/h, and 1.55 μR/h for G, G-10CRT, G-20CRT, and G-30CRT, respectively, for 100 keV. The higher $\frac{\mu_{en}}{\rho}$ values of CRT-rich geopolymer improved their dosimetry importance.

3.6. Buildup factors

The curves of EBF and EABF at different energies and selected mfps in G-xCRT are shown in Figs. 8 and 9, respectively. Quantitatively, the variations of EBF and EABF are the same. The buildup factors are greater for thicker samples due to multiple photon scattering. The buildup factors are higher at energies where ICS dominates photon interaction processes as a result of incoherent scattering of photons by the geopolymer samples. In addition, the buildup factors are greater than unity even for 1 mfp. This indicates that the thickness required for narrow beam transmission of photons through the prepared geopolymers is less than 1 mfp. At 1 and 40 mfp, EBFs of G, G-10CRT, G-20CRT, and G-30CRT are 1.07 and 1.27; 1.02 and 1.10; 1.02 and 1.07; and 1.01 and 1.06, respectively. Generally, the trend of EABF is G-10CRT > G > G-30CRT > G-20CRT while that of EBF is G > G-10CRT > G-30CRT > G-20CRT.

4. Conclusion

Metakaolin-based geopolymers were successively doped with CRT glass and investigated for their photon-shielding competence. The density of the composite geopolymer increased with the CRT glass content. The attenuation coefficients increased with CRT concentration. The HVL and mfp are within the ranges 0.070–18.079 cm and 0.101–26.083 cm for G; 0.036–15.110 cm and 0.052–21.799 cm for G-10CRT; 0.024–13.197 cm and 0.014–19.039 cm for G-20CRT; and 0.018–12.074 cm and 0.026–17.419 cm for G-30CRT. Samples rich in CRT had lower HVL and mfp at all energies. Z_{eff} was in the range 9.90–11.95, 10.34–23.22, 10.71–31.63, and 11.10–38.18, while the values of N_{eff} were within the range 2.98–3.63, 2.98–6.69, 2.98–8.80, and 2.98–10.24 $\times$ 10^{23} electron/g for G, G-10CRT, G-20CRT, and G-30CRT, respectively. The higher values of CRT-rich geopolymers improved their dosimetry importance. At 1 and 40 mfp, the EBFs of G, G-10CRT, G-20CRT, and G-30CRT were 1.07 and 1.27; 1.02 and 1.10; 1.02 and 1.07; and 1.01 and 1.06, respectively. Generally, the trend of EABF is G-10CRT > G > G-30CRT > G-20CRT, while that of EBF is G > G-10CRT > G-30CRT > G-20CRT. The introduction of CRT glass improved the shielding capacity of the metakaolin-based geopolymer. CRT-doped geopolymers are potentially useful for enhancing the radiation shielding potentials concrete. The infusion of CRT glass into geopolymers is an environmentally friendly way of recycling out-of-use CRT.

CRediT authorship contribution statement

M.S. Al-Buriahi: Conceptualization, Writing - Review and Editing. **Mine Kırkbınar:** Experimental work. **Z.A. Alrowaili:** Resources. **Khadijah Mohammedsaleh Katubi:** Support. **Norah Salem Alsaiari:** Support. **Amani Alalawi:** Resources. **Norah Alomayrah:** Project administration. **I.O. Olarinoye:** Writing - Original Draft.

Acknowledgement

The authors express their gratitude to Princess Nourah bint Abdulrahman University Researchers Supporting Project number (PNURSP2024R450), Princess Nourah bint Abdulrahman University, Riyadh, Saudi Arabia.

References

Al-Buriahi, Abouhaswa, A., Tekın, H., Sriwunkum, C., El-Agawany, F., Nutaro, T., Kavaz, E., & Rammah, Y. (2020). Structure, optical, gamma-ray and neutron shielding properties of NiO doped B2O3–BaCO3–Li2O3 glass systems. *Ceramics International, 46*(2), 1711–1721.

Al-Buriahi, Alomairy, S., & Mutuwong, C. (2021). Effects of MgO addition on the radiation attenuation properties of 45S5 bioglass system at the energies of medical interest: An in silico study. *Journal of the Australian Ceramic Society, 57*(4), 1107–1115.

Al-Buriahi, M. S., Alrowaili, Z. A., Alomairy, S., Olarinoye, I. O., & Mutuwong, C. (2022a). Optical properties and radiation shielding competence of Bi/Te-BGe glass system containing B2O3 and GeO2. *Optik, 257*, Article 168883.

Al-Buriahi, M. S., Alrowaili, Z. A., Eke, C., et al. (2022c). An important role of Ba2+, Sr2+, Mg2+, and Zn2+ in the radiation attenuation performance of CFCBPC bioactive glasses. *Journal of the Australasian Ceramic Society, 58*, 461–473.

Al-Buriahi, M. S., Alzahrani, J. S., Alrowaili, Z. A., Olarinoye, I. O., & Sriwunkum, C. (2023). Recycling of waste cathode-ray tube glasses as building materials for shielding structures in medical and nuclear facilities. *Construction and Building Materials, 376*, Article 131029.

Al-Buriahi, M. S., Gaikwad, D. K., Hegazy, H. H., Sriwunkum, C., & Neffati, R. (2021b). Fe-based alloys and their shielding properties against directly and indirectly ionizing radiation by using FLUKA simulations. *Physica Scripta, 96*(4), Article 045303.

Al-Buriahi, M. S., Kavas, T., Kavaz, E., Kurtulus, R., & Olarinoye, I. O. (2022b). Recycling potential of cathode ray tubes (CRTs) waste glasses based on Bi2O3 addition strategies. *Waste Management, 148*, 43–49.

Al-Buriahi, M. S., Sayyed, M. I., Bantan, R. A., & Al-Hadeethi, Y. (2021a). Nuclear radiation shielding characteristics of some natural rocks by using EPICS2017 library. *Materials, 14*(16), 4669.

Ali, H., Ghori, Z., Sheikh, S., & Gul, A. (2015). Effects of gamma radiation on crop production. *Crop production and global environmental issues*, 27–78.

Allen, R. G., Brown, F. A., Logie, L. C., Rovner, D. R., Wilson, S. G., & Zellmer, R. W. (1960). Acute effects of gamma radiation in primates. *Radiation Research, 12*(5), 532–559.

Almuqrin, A. H., Albarzan, B., Olarinoye, O. I., Kumar, A., Alwadai, N., & Sayyed, M. I. (2021). Mechanical and gamma ray absorption behavior of PbO-WO3-Na2O-MgO-B2O3 glasses in the low energy range. *Materials, 14*(13), 3466.

Alothman, M. A., Olarinoye, I. O., Sriwunkum, C., et al. (2022). Study of the radiation attenuation properties of MgO-Al2O3-SiO2-Li2O-Na2O glass system. *Journal of the Australasian Ceramic Society, 58*, 267–273.

Alrowaili, Z. A., Alnairi, M. M., Olarinoye, I. O., Alhamazani, A. A., Alshammari, G. S., & Al-Buriahi, M. S. (2023). Radiation attenuation of fly ash and rice husk ash-based geopolymers as cement replacement in concrete for shielding applications. *Radiation Physics and Chemistry*, Article 111489.

Alrowaili, Z. A., Alzahrani, J. S., Kırkbınar, M., İbrahimoğlu, E., Çalışkan, F., Olarinoye, I. O., … Al-Buriahi, M. S. (2023). Role of TiO2 addition on recycling of TV screen waste glasses: Experimental and theoretical studies on structure and radiation attenuation properties. *Ceramics International, 49*(17), 28022–28029.

Alshahrani, B., Alrowaili, Z. A., Alsufyani, S. J., Olarinoye, I. O., Mutuwong, C., & Al-Buriahi, M. S. (2022). Determining the optical properties and simulating the radiation shielding parameters of Dy3+ doped lithium yttrium borate glasses. *Optik, 250*, Article 168318.

Alshahrani, B., Olarinoye, I. O., Mutuwong, C., Sriwunkum, C., Yakout, H. A., Tekin, H. O., & Al-Buriahi, M. S. (2021). Amorphous alloys with high Fe content for radiation shielding applications. *Radiation Physics and Chemistry, 183*, Article 109386.

Alzahrani, F. M. A., Albarkaty, K. S., Çalişkan, F., Olarinoye, I. O., & Al-Buriahi, M. S. (2023). Physical, microstructural, and radiation energy absorption properties of recycled CRT-screen glass doped with Bi2O3. *Journal of Radiation Research and Applied Sciences, 16*(4), Article 100727.

Ardiansyah, A., Tahir, D., Heryanto, H., Armynah, B., Salah, H., Sulieman, A., & Bradley, D. A. (2023). Science mapping for concrete composites as radiation shielding: A review. *Radiation Physics and Chemistry*, Article 110835.

Asghar, R., Khan, M. A., Alyousef, R., Javed, M. F., & Ali, M. (2023). Promoting the green construction: Scientometric review on the mechanical and structural performance of geopolymer concrete. *Construction and Building Materials, 368*, Article 130502.

Basha, B., Kirkbinar, M., Katubi, K. M., İbrahimoğlu, E., Çalişkan, F., Olarinoye, I. O., … Al-Buriahi, M. S. (2024). Synthesis of Bi2O3 doping powder from CRT-screen waste glass: Physical, structural, and radiation attenuation properties. *Radiation Physics and Chemistry, 214*, Article 111279.

Bashter, I. (1997). Calculation of radiation attenuation coefficients for shielding concretes. *Annals of Nuclear Energy, 24*(17), 1389–1401.

Bawab, J., Khatib, J., Jahami, A., Elkordi, A., & Ghorbel, E. (2021). Structural performance of reinforced concrete beams incorporating cathode-ray tube (CRT) glass waste. *Buildings, 11*(2), 67.

Berger, M. J., & Hubbell, J. H. (1987). *XCOM: Photon cross sections on a personal computer* (No. NBSIR-87-3597). In *National Bureau of Standards*. Washington, DC (USA): Center for Radiation Research.

El-Ghazaly, M. A., Fadel, N. A., Abdel-Naby, D. H., Abd El-Rehim, H. A., Zaki, H. F., & Kenawy, S. A. (2020). Amelioration of adjuvant-induced arthritis by exposure to low dose gamma radiation and resveratrol administration in rats. *International Journal of Radiation Biology, 96*(7), 857–867.

Fernando, S., Gunasekara, C., Law, D. W., Nasvi, M. C. M., Setunge, S., & Dissanayake, R. (2023). Assessment of long term durability properties of blended fly ash-Rice husk ash alkali activated concrete. *Construction and Building Materials, 369*, Article 130449.

Gao, X., Yao, X., Xie, R., Li, X., Cheng, J., & Yang, T. (2022). Performance of fly ash-based geopolymer mortars with waste cathode ray tubes glass fine aggregate: A comparative study with cement mortars. *Construction and Building Materials, 344*, Article 128243.

Gerward, L., Guilbert, N., Jensen, K. B., & Levring, H. (2004). WinXCom—a program for calculating X-ray attenuation coefficients. *Radiation Physics and Chemistry, 71*(3–4), 653–654.

Górski, M., Wielgus, N., Loska, K., Kozioł, M., Landrat, M., Ścierski, W., & Pikoń, K. (2021). Characteristics of metakaolin-based geopolymer with cathode ray tube glass. *Polymers, 13*(7), 1149.

Güler, S. H., Güler, Ö., Kavaz, E., ALMisned, G., Albayrak, M. G., Issa, B., & Tekin, H. O. (2024). Fabrication and structural, physical, and nuclear radiation shielding properties for Oxide Dispersion-Strengthened (ODS) alloys through Erbium (III) oxide, Samarium (III) oxide, and Praseodymium (III) oxide into 316L matrix. *Ceramics International, 50*(3), 5443–5452.

Günoğlu, K., Akkurt, I., & Sayyed, M. I. (2024). Radiation shielding properties of some igneous rocks in isparta province at different gamma energies: Experimental and theoretical study. *Journal of Radiation Research and Applied Sciences, 17*(1), Article 100796.

Guzmán-Carrillo, H. R., Gasca-Tirado, J. R., López-Romero, J. M., Luis, M. A. C., Eric, M. R. M., Pineda-Piñón, J., … Manzano-Ramírez, A. (2021). Encapsulation of toxic heavy metals from waste CRT using calcined kaolin base-geopolymer. *Materials Chemistry and Physics, 257*, Article 123745.

Hornitzky, M. A. (1994). Commercial use of gamma radiation in the beekeeping industry. *Bee World, 75*(3), 135–142.

Hwalla, J., Bawab, J., El-Hassan, H., Abu Obaida, F., & El-Maaddawy, T. (2023). Scientometric analysis of global research on the utilization of geopolymer composites in construction applications. *Sustainability, 15*(14), Article 11340.

Hwang, C. L., & Huynh, T. P. (2015). Effect of alkali-activator and rice husk ash content on strength development of fly ash and residual rice husk ash-based geopolymers. *Construction and Building Materials, 101*, 1–9.

Kang, S., Lee, H. J., Son, Y., Bae, M. J., Jo, W. S., Park, J. H., … Kim, J. S. (2023). Low-dose-rate gamma radiation aggravates titanium dioxide nanoparticle-induced lung injury in mice. *Molecular & Cellular Toxicology*, 1–10.

Katiyar, P., Pandey, N., & Keshavkant, S. (2022). Gamma radiation: A potential tool for abiotic stress mitigation and management of agroecosystem. *Plant Stress, 5*, Article 100089.

Katubi, K. M., Olarinoye, I. O., Alrowaili, Z. A., & Al-Buriahi, M. S. (2022). Optical transmission, polarizability, and photon/neutron shielding properties of Bi2O3/MnO/B2O3 glass system. *Optik, 268*, Article 169695.

Kaur, T., Sharma, J., & Singh, T. (2019). Review on scope of metallic alloys in gamma rays shield designing. *Progress in Nuclear Energy, 113*, 95–113.

Long, W. J., Zhang, X., Xie, J., Kou, S., Luo, Q., Wei, J., … Feng, G. L. (2022). Recycling of waste cathode ray tube glass through fly ash-slag geopolymer mortar. *Construction and Building Materials, 322*, Article 126454.

Madureira, J., Dias, M. I., Pinela, J., Calhelha, R. C., Barros, L., Santos-Buelga, C., … Verde, S. C. (2020). The use of gamma radiation for extractability improvement of bioactive compounds in olive oil wastes. *Science of the Total Environment, 727*, Article 138706.

Mansoori, E., Morshedian, J., & Darounkola, M. R. R. (2023). Elaboration of X-ray shielding of highly barite-loaded polyester concrete: Structure, mechanical properties, and MCNP simulation. *Construction and Building Materials, 370*, Article 130650.

Mansour, M., Bedjaoui, W., & Trari, M. (2024). Effect of γ-rays irradiation on optical and structural properties of the perovskite 128° Y-cut LiNbO3 single crystal. *Nuclear Instruments and Methods in Physics Research Section B: Beam Interactions with Materials and Atoms, 547*, Article 165206.

Maschio, S., Tonello, G., & Furlani, E. (2013). Recycling glass cullet from waste CRTs for the production of high strength mortars. *Journal of Waste Management, 2013*.

Mikhalkevich, N., O'Carroll, I. P., Tkavc, R., Lund, K., Sukumar, G., Dalgard, C. L., … Iordanskiy, S. (2021). Response of human macrophages to gamma radiation is mediated via expression of endogenous retroviruses. *PLoS Pathogens, 17*(2), Article e1009305.

Mohamed, N. A., Kiong, T. S., Ismail, A. F., & Teridi, M. A. M. (2024). Novel gamma-ray enhanced TiO2 nanoparticles photoanode for efficient photoelectrochemical (PEC) water splitting. *Applied Surface Science, 642*, Article 158602.

Nawaz, M., Heitor, A., & Sivakumar, M. (2020). Geopolymers in construction-recent developments. *Construction and Building Materials, 260*, Article 120472.

Ogundare, F. O., Olarinoye, I. O., & Obed, R. I. (2008). Estimation of patients' organ doses and conceptus doses from selected X-ray examinations in two Nigeria X-ray centres. *Radiation Protection Dosimetry, 132*(4), 395–402.

Ogundiran, M. B., & Enakerakpo, I. S. (2018). Metakaolin clay-derived geopolymer for recycling of waste cathode ray tube glass. *African Journal of Pure and Applied Chemistry, 12*(6), 42–49.

Olarinoye, I. O. (2017). *Photon buildup factors for some tissues and phantom materials for penetration depths up to 100 MFP*.

Olarinoye, I. O., Odiaga, R. I., & Paul, S. (2019). EXABCal: A program for calculating photon exposure and energy absorption buildup factors. *Heliyon, 5*(7), Article e02017.

Podgoršak, E. B. (2006). *Radiation physics for medical physicists* (Vol. 1). Berlin: Springer.

Pricaz, M. A. R. I. A., & Uță, A. C. (2015). Gamma radiation for improvements in food industry, environmental quality and healthcare. *Romanian Journal of Biophysics, 25*(2), 143–162.

Roshani, M., Phan, G., Faraj, R. H., Phan, N. H., Roshani, G. H., Nazemi, B., … Nazemi, E. (2021). Proposing a gamma radiation based intelligent system for simultaneous analyzing and detecting type and amount of petroleum by-products. *Nuclear Engineering and Technology, 53*(4), 1277–1283.

Shaaban, K. S., Abo-Naf, S. M., & Hassouna, M. E. M. (2019). Physical and structural properties of lithium borate glasses containing MoO3. *Silicon, 11*, 2421–2428.

Ślosarczyk, A., Fořt, J., Klapiszewska, I., Thomas, M., Klapiszewski, Ł., & Černý, R. (2023). A literature review of the latest trends and perspectives regarding alkali-activated materials in terms of sustainable development. *Journal of Materials Research and Technology*.

Vucic, V., Isenovic, E. R., Adzic, M., Ruzdijic, S., & Radojcic, M. B. (2006). Effects of gamma-radiation on cell growth, cycle arrest, death, and superoxide dismutase

expression by DU 145 human prostate cancer cells. *Brazilian Journal of Medical and Biological Research, 39*, 227–236.
Yoshida, Y. (2006). Development of fitting methods using geometric progression formulae of gamma-ray buildup factors. *Journal of Nuclear Science and Technology, 43* (12), 1446–1457.
Zhang, P., Sun, X., Wang, F., & Wang, J. (2023). Mechanical properties and durability of geopolymer recycled aggregate concrete: A review. *Polymers, 15*(3), 615.